ELSEVIER

Chemical Engineering Science 62 (2007) 7163–7171

Chemical Engineering Science

www.elsevier.com/locate/ces

Oxygen transfer prediction in aeration tanks using CFD

Yannick Fayolle[a], Arnaud Cockx[b], Sylvie Gillot[a,*], Michel Roustan[b], Alain Héduit[a]

[a] *Cemagref, Unité HBAN, Parc de Tourvoie, BP 44, 92163 Antony Cedex, France*
[b] *LISPB, Complexe scientifique de Rangueil, 31077 Toulouse Cedex 4, France*

Received 20 April 2007; received in revised form 13 July 2007; accepted 12 August 2007
Available online 4 September 2007

Abstract

In order to optimize aeration in the activated sludge processes, an experimentally validated numerical tool, based on computational fluid dynamics and able to predict flow and oxygen transfer characteristics in aeration tanks equipped with fine bubble diffusers and axial slow speed mixers, is proposed. For four different aeration tanks (1;1493;8191 and 29, 313 m^3), this tool allows to precisely reproduce experimental results in terms of axial liquid velocities, local gas hold-ups. Predicted oxygen transfer coefficients are within ±5% of experimental results for different operating conditions (varying pumping flow rates of the mixers and air flow rates). The actual bubble size must be known with precision in order to have a reliable estimation of the oxygen transfer coefficients.

Keywords: Aeration; Multiphase flow; Mass transfer; Hydrodynamics; Bubble; Wastewater treatment

1. Introduction

In urban wastewater treatment, the main process to treat nitrogen and organic components of wastewater is the activated sludge one. Aeration in this process can represent up to 70% of the total energy expenditure of the plant. Optimizing aeration is therefore required to reduce operating costs, in addition to guaranty a reliable and efficient treatment in such installations. Since the last 20 years, fine bubble aeration systems have been extensively implemented to perform aeration. They proved to give high oxygenation performances, and to be adaptive to oxygen requirements. For loop reactors commonly installed in Europe, fine bubble aeration is separated from mixing, carried out by axial slow speed mixers. Numerous on site results pointed out the main parameters impacting oxygen transfer (Groves et al., 1992; Wagner and Pöpel, 1998; Gillot et al., 2000; Mueller et al., 2002). However, oxygen transfer in deep aeration tanks remains difficult to predict (Gillot et al., 2005). This may be due to the parameters that are not taken into account in the analysis of the experimental results (bubble size, gas hold-up, local axial velocity). More precise information on the local hydrodynamics of aeration tanks is therefore necessary in order to better understand the impact of design and operating parameters on oxygen transfer.

In addition, computational fluid dynamics (CFD) is more and more used to optimize aeration systems (Simon, 2000; Cockx et al., 2001; Vermande et al., 2003, 2005). Previously introduced by Chatellier (1991) and Simon (2000), the modelling of monophasic flows in aeration tanks induced by axial slow speed mixers was studied by Vermande et al. (2003). These authors showed that the modelling of axial slow speed mixers by imposing the characteristics of the flow induced by agitation, on a zone of the grid corresponding to the location of the mixer (fixed values method), gives a good prediction of the mean experimental axial liquid velocity.

In Cockx et al. (2001), ASTRID code was used to analyse bubble interfacial area on a full scale aeration tank (15,000 m^3). The structure of the flow was shown to be tri-dimensional and composed of large recirculation movements of liquid resulting from mutual interaction between bubble plumes. However, this numerical study was not confronted to experimental results which would have allowed validating the CFD results. Moreover, the size of the bubbles was empirically imposed and considered as constant in the entire tank. The impact of this hypothesis has therefore to be investigated.

Finally, Vermande et al. (2005) recently investigated the behaviour of two-phase flows in a full scale aeration tank

* Corresponding author. Tel.: +33 1 40 96 60 66; fax: +33 1 40 96 61 99.
E-mail address: sylvie.gillot@cemagref.fr (S. Gillot).

0009-2509/$ - see front matter © 2007 Elsevier Ltd. All rights reserved.
doi:10.1016/j.ces.2007.08.082

Table 1
Dimensions and equipment description of the studied aeration tanks (diffuser grid placement and mixers are represented on the schematic representation)

Tank	Type	Geometry and diffuser grid placement	Volume (m^3)	Dimensions	Mixers	Air supply	
						Number of diffuser grids	Number of diffuser on each grid
1	Oblong		1	$L = 3$ m; $l = 1$ m; $d_w = 0.4$ m	One axial mixer ($D = 0.15$ m)	–	1
2	Annular	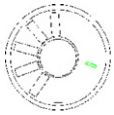	1493	$D_{out} = 20.25$ m; $D_{in} = 7.83$ m; $d_w = 5.45$ m	One large blade slow speed mixer ($D = 2.5$ m)	6	26
3	Oblong	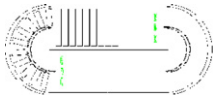	8191	$L = 50.65$ m; $l = 27.5$ m; $d_w = 5.3$ m	Six large blades slow speed mixer (four of $D = 2.5$ m and two of $D = 2.2$ m)	18 and 10	88 and 44
4	Oblong	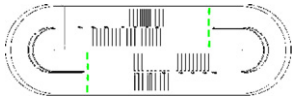	29,313	$L = 90.63$ m; $l = 34.08$ m; $d_w = 8.6$ m	Eight large blades slow speed mixers ($D = 2.4$ m)	24	87

Table 2
Bubble Sauter diameter at $P = 1.013 \times 10^5$ Pa introduced in each simulation (where Q_{diff} is the mean air flow rate per diffuser and d_{bs} is the bubble Sauter diameter)

Tank	1				2		3	4
Q_{diff} ($Nm^3 h^{-1}$)	2.58		3.25		9.97		4.75	6.06
U_C ($m s^{-1}$)	0.10	0.30	0.10	0.30	0.00	0.42	0.15	0.23
d_{bS} (mm)	1.93	2.70	1.99	2.62	4.94	4.77	4.27	4.60

Table 3
Number of cells of the grid for each one of studied aeration tanks

Tank	1	2	3	4
Volume (m^3)	1	1493	8191	29,313
Number of cells	29,147	13,266	128,704	452,440

($6200\ m^3$). Unfortunately, no experimental validation of the computed results and no complete description of the models and of the closure relations implemented to simulate two-phase flow have been presented by the authors.

The objective of this paper is therefore to present an experimentally validated numerical tool able to predict flow and oxygen transfer characteristics in aeration tanks equipped with fine bubble diffusers and axial slow speed mixers. Models used to this aim are described and analysed. The impact of the bubble size used to perform the simulations is also investigated.

2. Materials and methods

2.1. Experimental set-up

Four aeration tanks from pilot scale to full scale have been analysed. These tanks (1–29,313 m^3) are closed loop reactors in which aeration is separated from mixing, carried out by axial slow speed mixers. Air is injected at the bottom of the tank through EPDM (Ethylene–Propylene Diene Rubber) membrane diffusers (fine bubbles) arranged in several separated grids. The main characteristics of the basins are summarized in Table 1.

In the pilot plant (tank 1), experimental results (axial liquid velocity, bubble size, local gas hold-up and oxygen transfer coefficient) were obtained by Simon (2000).

Axial liquid velocity, bubble size and oxygen transfer coefficient measurements have been performed on each full scale aeration tanks in this work. The *in situ* measurement methods have been described in detail in a previous paper (Fayolle et al., 2006).

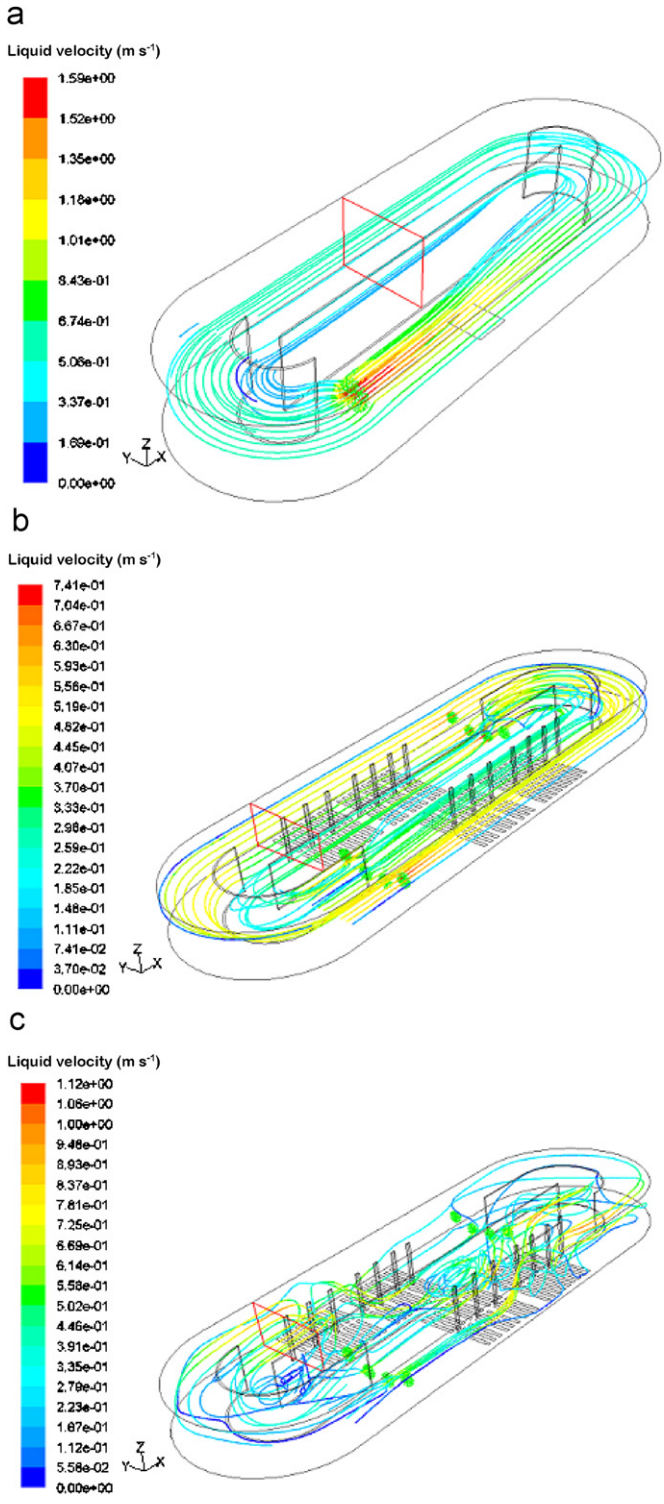

Fig. 1. Streamlines coloured by velocity magnitude ($m\,s^{-1}$) (a) in tank 1 without aeration ($Q_T = 0\,Nm^3\,h^{-1}$; $U_C = 0.35\,m\,s^{-1}$) (b) in tank 4 without aeration ($Q_T = 0\,Nm^3\,h^{-1}$; $U_C = 0.27\,m\,s^{-1}$) and (c) in tank 4 with aeration ($Q_T = 12,653\,Nm^3\,h^{-1}$; $U_C = 0.23\,m\,s^{-1}$).

2.2. Mathematical modelling

Flow and oxygen transfer computations were determined with the 6.2 version of the CFD code FLUENT. This code uses the finite volume method for the discrimination of the Navier–Stokes equations. When turbulent flows are considered, such as in aeration tanks, the modelling of the bubbly flow is based on the Eulerian two-fluid model derived from Reynolds average Navier–Stokes equations. This model is generally used to simulate bubbly flow reactors with a large number of bubbles (Cockx et al., 1999; Vermande et al., 2005; Talvy et al., 2007). For example, in an aeration tank of 1 m^3, a global gas hold-up of 1% represents around 700,000 bubbles. For industrial aeration tanks, it seems difficult to calculate the movement of each inclusion by an Eulerian–Lagrangian model. The Euler–Euler model is then selected in order to describe the average movement of inclusions. The development of this model is now classical (Ishii, 1975). Only principal models used to simulate flow and oxygen transfer characteristics are briefly described in the following.

2.2.1. Two-phase hydrodynamics

The two-phase flow mass conservation equations for each phase are considered as follows:

$$\frac{\partial \rho_k \alpha_k}{\partial t} + \vec{\nabla}.(\alpha_k \rho_k \vec{v}_k) = 0. \tag{1}$$

The equations of conservation of momentum are

$$\frac{\partial \alpha_k \rho_k \vec{v}_k}{\partial t} + \vec{\nabla}.(\alpha_k \rho_k \vec{v}_k \otimes \vec{v}_k) = -\vec{\nabla}(\alpha_k P_k) + -\vec{\nabla}(\alpha_k \bar{\bar{\tau}}_k) + \overline{M}_k + \alpha_k \rho_k \vec{g}, \tag{2}$$

where P_k is the pressure of phase k and $\overline{M}_k = \alpha_k \rho_k \sum \overline{F}$ represents the interfacial transfer of momentum due to pressure and viscous stress distribution and $\sum \overline{F}$ represents the sum of the forces exerted on an inclusion. In the case of a gas/liquid reactor, the interfacial transfer of momentum is principally influenced by the drag force F_D, the weight and the buoyant force. The interfacial transfer of momentum related to drag is expressed as follows:

$$F_D = \tfrac{1}{2} \rho_k A_p C_D |\overline{V_r}| \overline{V_r}, \tag{3}$$

where $\overline{V_r}$ represents the relative velocity, C_D is the drag coefficient and A_p is the projected interfacial area. The drag coefficient used in the present work was proposed by Clift et al. (1978) and is expressed as

$$C_D = \tfrac{2}{3}\sqrt{Eo}, \tag{4}$$

where $Eo = (\rho_L - \rho_G) g d_b^2 / \sigma$ is the Eötvos number.

This correlation is adapted to the modelling of drag coefficients for gas bubbles. The rise velocity is well represented with this correlation for the range of studied bubble size (from 3.0 to 5.5 mm). This correlation takes into account the ellipsoidal shape of bubbles (for a bubble size of 4.0 mm, the drag coefficient is of 0.98 by the correlation of Clift et al. (1978) and of 0.44 by the correlation of Schiller and Naumann (1938), developed for rigid sphere).

The k–ε dispersed model is used in order to model the turbulence. This model considers that bubble–bubble and

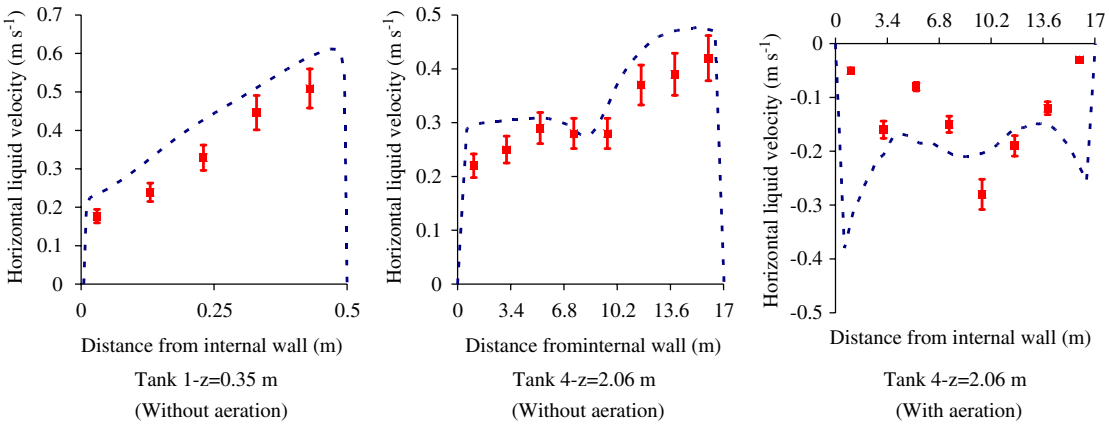

Fig. 2. Axial liquid velocity ($m\,s^{-1}$) versus distance from internal wall (m) (■, experimental; —, CFD). z represents the distance from the bottom of the tank (m).

bubble–wall collisions are negligible and the dominant process in the random motion of the secondary phases is the continuous phase turbulence. So, a k–ε model and the Tchen-theory correlations (Hinze, 1975) are respectively applied to the continuous and dispersed phase. The term $\overrightarrow{v_d}$, the drift velocity (Bel Fdhila and Simonin, 1992), is introduced in the expression of the relative velocity $\overrightarrow{V_r}$ in order to express the interface turbulent momentum transfer. So, the relative velocity $\overrightarrow{V_r}$ is modelled as follows:

$$\overrightarrow{V_r} = \overrightarrow{v_G} - \overrightarrow{v_L} - \overrightarrow{v_d}. \tag{5}$$

The dispersion of the gas phase transported by the turbulent fluid motion must be taken into account in FLUENT by activating the drift velocity model. Drift velocity is essential to well simulate the gas hold-up (Talvy et al., 2007).

2.2.2. Two-phase mass transfer

To reproduce the experimental set-up of oxygen transfer coefficient measurements, two scalars (quantity that is affected by the flow without itself affecting the flow) must be introduced to represent oxygen concentration in each phase. The general transport equations of the concentration of these scalars in two-phase flows are expressed as

$$\frac{\partial \alpha_k c_k}{\partial t} + \vec{\nabla}.(\alpha_k c_k \vec{v}_k) = -\vec{\nabla}.(\alpha_k(\vec{J}_k + \overline{c'_k v'_k})) + \overline{L_k}, \tag{6}$$

where $\overline{L_k}$ represents the interfacial transfer of concentration, J_k is the flux due to the molecular diffusion and $\overline{c'_k v'_k}$ represents the turbulent diffusion of the concentration.

The oxygen mass transfer between the gas bubble and the liquid is modelled as follows:

$$\overline{L_L} = k_L a(C_L * - C_L), \tag{7}$$

where a is the interfacial area, k_L is the local mass transfer coefficient and $(C_L * - C_L)$ is the driven force of the oxygen transfer. The saturation concentration C_L* in water depends on local pressure according to Henry's law:

$$C_L * = \frac{y_e P_G}{He} = m C_G, \tag{8}$$

where y_e is the volume fraction of oxygen in air, P_G is the pressure in the bubble, m is a coefficient linked to Henry's coefficient (He) and C_G is the concentration of oxygen in the bubble. The interfacial area is defined as the ratio of the total air bubble surface and the volume of liquid. For spherical bubbles having a bubble Sauter diameter d_{bS}, the interfacial area is expressed as

$$a = \frac{6}{d_{bS}} \frac{\alpha_G}{1 - \alpha_G}. \tag{9}$$

Finally, the local mass transfer coefficient is modelled using the classical penetration theory (Higbie, 1935):

$$k_L = 2\sqrt{\frac{D_L V_r}{\pi d_b}}, \tag{10}$$

where D_L is the diffusion coefficient of the oxygen in water (at 20 °C).

2.2.3. Boundary conditions

The boundary conditions relate to the injection of the gas, the bubble size, the mixing modelling and the modelling of the free surface.

Surfaces of gas injection correspond to the total area covered by the modules of bubble diffusers. These surfaces do not take into account each one of the diffusers individually but the entire grid. The injected air flow rate corresponds to the air flow rate at the pressure of the diffuser submergence. The oxygen concentration in the injected bubbles is expressed as

$$C_G = \frac{y_e . M_{O_2} . P_G}{RT}, \tag{11}$$

where y_e is the volume fraction of oxygen in air, M_{O_2} is the molecular mass of the oxygen, R is the gas constant, T is the temperature and P_G is the pressure at the diffuser level.

The initial bubble size (just above the diffusers) is determined from experimental results. Bubble sizes (at $P = 1.013 \times 10^5$ Pa) introduced in each simulation are summarized in Table 2.

In order to reproduce the experimental data, the bubble size is expressed as a function of the hydrostatic pressure

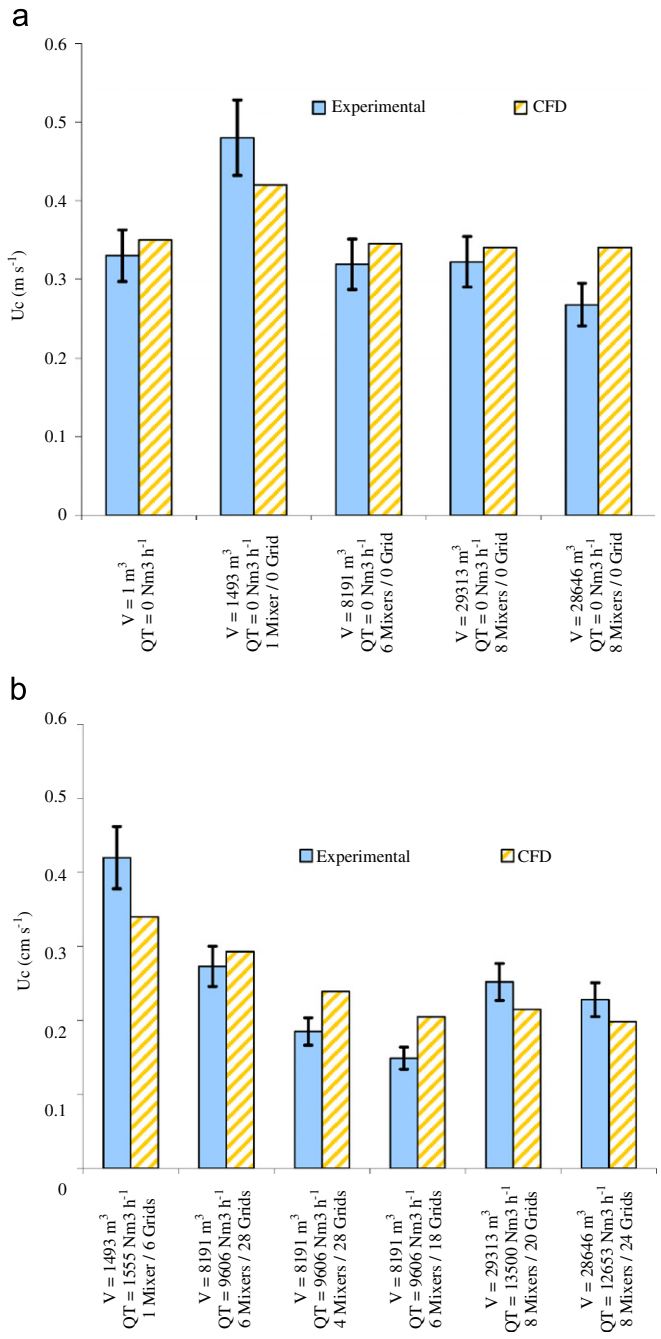

Fig. 3. Axial liquid velocities for each basin and whatever operating conditions (a) *without* aeration and (b) *with* aeration. (■, experimental; □, CFD).

(Fayolle et al., 2006). The coalescence and rupture phenomena are not taken into account in the evolution because of the low average gas hold-up in the aerated tank. The consumption of oxygen contained in bubbles during their rising is considered to have any effect on their size (Jupsin and Vasel, 2002).

Mixing is modelled by the fixed value method validated by Vermande et al. (2003). This method consists in simplifying the numerical resolution by ignoring the flow equations crossing the agitator and considering the mixers as a source of momentum. Characteristics of the flow induced by agitation are imposed on a zone of the grid corresponding to the location of the mixer. Moreover, no boundary condition concerning turbulence is imposed (Chatellier, 1991; Djebbar, 1996).

The free surface is modelled by a degasification condition for the gas phase and a symmetry condition for the liquid phase. In this case, the surface is considered as mobile, strengthless and horizontal. The oxygen transfer from the free surface is neglected in comparison to the bubble interfacial area. Indeed, the order of magnitude of bubble/liquid interfacial area ($a_b = 3$–$10\,\mathrm{m}^{-1}$) is more important than the free surface interfacial area ($a_S = \frac{S_T}{V_T} = \frac{1}{d_w}$), particularly for deep aeration tanks.

Finally, all simulations have been performed in clean water ($\rho_L = 1000.0\,\mathrm{kg\,m^{-3}}$; $\mu_L = 1.0 \times 10^{-3}\,\mathrm{kg\,m^{-1}\,s^{-1}}$) and the flow is assumed to be isothermal (the simulations take place with water and air at $T = 20\,^{\circ}\mathrm{C}$).

2.2.4. Mesh grid

The flow structure in aerated tanks is three-dimensional (Cockx et al., 2001). For each studied tanks, 3D grid meshes have been created (using the pre-processor GAMBIT). All meshes are unstructured and composed of tetrahedrons. The number of cells of resulting grids are summarized in Table 3. The grid has been refined near the wall for the pilot scale aeration tank to simulate precisely the flow characteristics. The size of the grid is sufficient to have a grid-independent solution.

3. Comparison of CFD and experimental results

Axial liquid velocity, gas hold-up profiles and oxygen transfer coefficients obtained by CFD are compared with the experimental results.

3.1. Axial liquid velocity

3.1.1. Axial liquid velocity profiles

The axial liquid velocity profiles have been measured in a non-aerated experimental section using a mono-directional flow-meter.

Fig. 1 represents simulated streamlines respectively in tank 1 without aeration, and in tank 4 without and with aeration. The red rectangle represents the section of experimental axial velocity measurement.

The flow in aeration tanks is mainly axial without aeration (Fig. 1(a) and (b)). However, with aeration, the streamlines are deformed by the gas injection (Fig. 1(c)). Zones of recirculation due to the drag of the liquid by the gas phase (spiral flows) are observed in the aerated zone. Spiral flows are also observed near the internal wall downstream from the bends.

Table 4
Measurement section area of axial velocity, number of measurement points and the ratio between the number of measurement points and measurement section area

Tank	1	2	3	4
Measurement section area (m^2)	0.2	33.8	70.2	142.2
Number of measurement points	20	35	30	48
Number of points/m^2 of measurement section	100.0	1.0	0.4	0.3

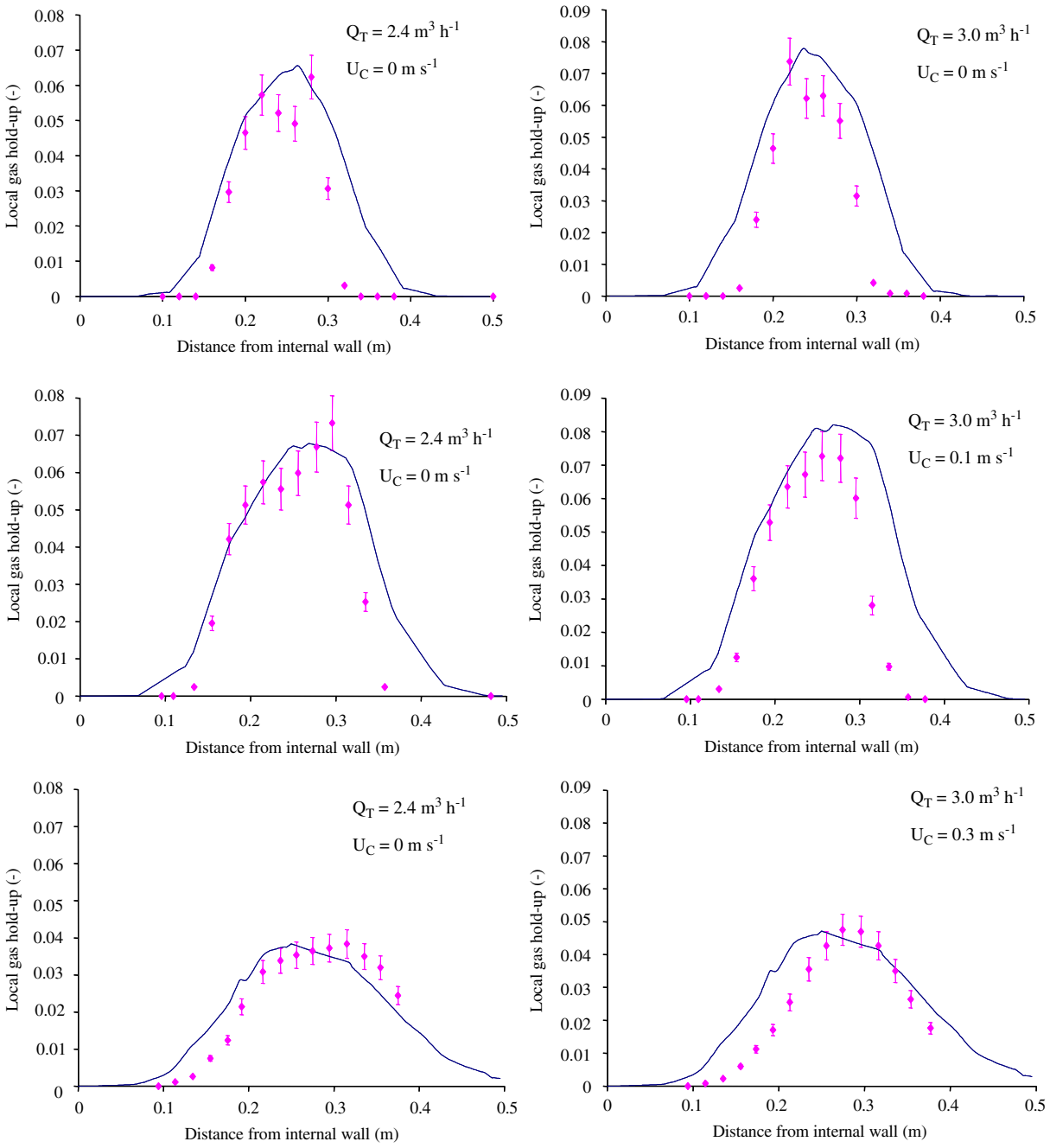

Fig. 4. Transverse gas hold-up profile for different air flow rates (Q_T) and mean axial liquid velocity (U_C). ♦ experimental data / - numerical data.

Fig. 2 presents the evolution of local axial liquid velocities versus the distance from the internal wall for tanks 1 (1 m^3) and 4 (29, 313 m^3). Velocity profiles without (tanks 1 and 4) and with aeration (tank 4) are presented for a distance from the bottom of the tank (z) of 0.35 m (tank 1) and 2.06 m (tank 4). Velocity measurement sections are located away from the mixers.

For pilot and full scale basins, axial liquid velocity profiles measured without and with aeration are well predicted by the model.

For tank 1 without aeration, the experimental axial liquid velocity increases from 0.18 to 0.51 m s^{-1} with the distance from the internal wall. The experimental heterogeneity of the local axial velocity is well predicted by the model.

For tank 4 without aeration, the axial liquid velocity varies from 0.22 to 0.42 m s^{-1} with the distance from the internal wall. The axial liquid velocity profile is relatively homogenous on the measurement section and is well reproduced by simulation.

For tank 4 with aeration, the axial liquid velocity varies from -0.28 to -0.03 m s^{-1} with the distance from the internal wall. With aeration, the axial liquid velocity profile is strongly impacted when the flow crosses the bubble plume (the measurement section is placed downstream from this plume). The numerical simulation also allows to determine the order of

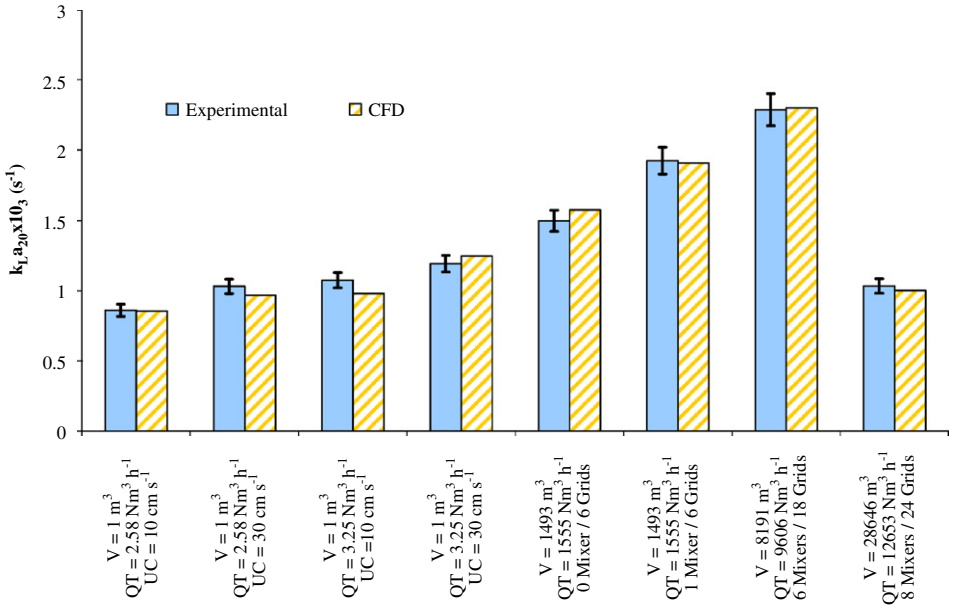

Fig. 5. Oxygen transfer coefficient for each basin and operating conditions (■, experimental; □, CFD).

Table 5
Oxygen transfer coefficient as a function of the input bubble Sauter diameter

Bubble Sauter diameter at $P = 1013$ hPa (mm)	4.29	4.77	5.25
$k_La_{20} \times 10^3$ (s^{-1})	2.19	1.91	1.71
Variation/$d_b = 4.77$ mm (%)	15	–	−11

magnitude of local axial liquid velocities. However, differences between experimental and CFD results on full scale aeration tank are more important than those observed on pilot scale tank. This may be due to the placement of the measurement probe which is not known with precision on full scale aeration tank. A measurement error related to the position of the probe should be added to the sampling error which is indicated in Fig. 2.

3.1.2. Mean axial liquid velocity

The good prediction of the local axial liquid velocities induces a reliable determination of the mean axial liquid circulation velocity, which is deduced by integration of the axial components of the velocity vector on the measurement surface. The experimental mean axial liquid velocity is calculated as the arithmetic average of the velocities measured on the experimental section. The results without and with aeration are summarized in Fig. 3. An axial velocity measurement error of 10% has been previously determined on full scale tank (Fayolle et al., 2006) and is indicated in Fig. 3.

Without aeration, the mean horizontal velocity is well predicted (differences between experimental and numerical data are about 10%) for each studied tank and whatever the operating conditions. With aeration, the difference between experimental and numerical data is more important. This difference could be mainly due to the difficult estimation of the pumping flow rate of the mixers. The influence of the aeration on this flow rate is indeed neglected. The observed difference could also be due to a number of experimental points which was certainly insufficient to determine the mean axial velocity. A previous study (Fayolle, 2006) showed that one measurement point per square meter of section was necessary to determine precisely this value. The number of measurement points for tanks 3 and 4 was lower than this recommendation (Table 4).

3.2. Gas hold-up

For the pilot scale aeration tank, the computed gas hold-up profiles are compared to experimental local measurements using an optical probe (Simon, 2000). Simulations are performed for two different air flow rates ($Q_T = 2.4$ and $3.0\,m^3\,h^{-1}$) and three different axial liquid velocities (U_C=0, 0.1 and 0.3 m s^{-1}) corresponding to the experimental operating conditions. The results in terms of transversal gas hold-up profiles (at $z = 0.18$ m from the diffusers) are summarized in Fig. 4.

A good agreement between experimental and numerical gas hold-up profiles is obtained whatever the operating conditions, in the pilot scale aeration tank. The differences observed between numerical and experimental gas hold-up profiles on the pilot aeration tank probably result from:

- the numerical gas injection that is numerically realized on the total surface of the diffusers and not only on the experimental perforated zones of the diffusers;
- the experimental position of the probe which is not clearly defined (“in the centre of the bubble plume”, Simon, 2000).

3.3. Oxygen transfer

When the oxygen transfer is simulated, the dissolved oxygen concentration in the liquid phase is plotted versus time at several locations corresponding to the experimental placement of the dissolved oxygen probes. The apparent oxygen transfer

coefficient (k_La) is determined by fitting the curve with the following exponential function, based on the perfectly mixed reactor hypothesis (NF-EN-12255-15, 2004):

$$C_L = C_S - (C_S - C_0)\,\mathrm{e}^{-k_La_{20}t}, \tag{12}$$

where C_L is the dissolved oxygen (DO) concentration in water, C_0 is the initial DO concentration in water, C_S is the DO concentration in water at the saturation and k_La_{20} is the oxygen transfer coefficient at $T = 20\,^{\circ}\mathrm{C}$.

The oxygen transfer coefficients are deduced from experimental and simulated evolution of the oxygen concentration in the liquid versus time. The obtained coefficients are reported in Fig. 5.

For both pilot and full scale tanks, the oxygen transfer coefficient is well predicted by simulation whatever the operating conditions (difference between experimental and computed data lower than 5%). The simulation of two-phase flows, coupled with oxygen transport for each phase, allows to determine precisely the oxygen transfer coefficient of full scale aeration tanks by taking into account the complex and competitive effects of the pressure.

3.4. Influence of the bubble size on the computed oxygen transfer coefficient

The bubble size is the dominating parameter in oxygen transfer phenomena, as, together with the gas hold-up, it governs the interfacial area. During CFD simulation, the global gas hold-up is computed whereas the bubble size is an input parameter. A sensitivity analysis of the CFD results to the input bubble size was therefore realized on tank 2. The input bubble Sauter diameter was modified by ±10% from the experimental value. The computed global oxygen transfer coefficients are shown in Table 5.

A decrease in the bubble size of 10% induces an increase in the oxygen transfer coefficient by 15%. Inversely, increasing the bubble diameter by 10% induces a decrease in the oxygen transfer coefficient (−11%). The evolution of k_La_{20} with d_{bs} is not linear because an increase in the bubble size has two main impacts: (i) an increase in the local interfacial area and (ii) an increase in the local mass transfer coefficient. These results confirm the necessity to measure *in situ* the air bubble diameter. Adequate tools to estimate and model the bubble size at the diffuser level are required to overcome this issue.

4. Conclusions

A numerical tool to simulate flow characteristics and oxygen transfer in aeration tanks has been presented. The proposed protocol includes the main numerical models to be used, especially concerning the drag force and the drift velocity. This tool has been validated by comparison of measured and computed data in terms of axial liquid velocity, local gas hold-up and oxygen transfer coefficient for four tanks of different sizes (pilot and full scale). The axial liquid velocities and the gas hold-up profiles are well predicted by the model. Moreover, the apparent oxygen transfer coefficient is precisely reproduced with an accuracy of 5%. The proposed protocol allows taking into account the complex and competitive effects of the pressure, principally on the bubble size along their rise. This validated model will be used to predict and to optimize oxygenation capacities of full scale tanks. However, the predicted accuracy is dependant of the inlet bubble size value.

Notation

a	bubble interfacial area, m^{-1}
A_p	projected interfacial area, m^2
c_k	local instantaneous scalar concentration in phase k, $\mathrm{kg\,m}^{-3}$
c'_k	local instantaneous turbulent component of scalar concentration in phase k, $\mathrm{kg\,m}^{-3}$
C_0	initial dissolved oxygen (DO) concentration in water, $\mathrm{kg\,m}^{-3}$
C_D	drag coefficient, dimensionless
C_G	concentration of oxygen in the bubble, $\mathrm{mg\,l}^{-1}$
C_L	DO concentration in water, $\mathrm{kg\,m}^{-3}$
C_L*	instantaneous DO concentration at the gas-liquid interface, $\mathrm{kg\,m}^{-3}$
C_S	DO concentration at the saturation, $\mathrm{kg\,m}^{-3}$
d_b	bubble diameter, m
d_{bS}	bubble Sauter diameter, m
d_w	water depth, m
D_L	diffusion coefficient of the oxygen in the water, $\mathrm{m}^2\,\mathrm{s}^{-1}$
Eo	Eötvos number, dimensionless
F_D	drag force, $\mathrm{kg\,m\,s}^{-2}$
g	gravitational acceleration constant, $\mathrm{kg\,m}^{-2}$
He	Henry's coefficient, $\mathrm{Pa\,m}^3\,\mathrm{kg}^{-1}$
J_k	flux due to molecular diffusion, $\mathrm{mol\,s}^{-1}\,\mathrm{m}^{-2}$
k_L	local mass transfer coefficient, $\mathrm{m\,s}^{-1}$
k_La_{20}	oxygen transfer coefficient in standard conditions ($P = 1.013 \times 10^5$ Pa and $T = 20°\mathrm{C}$), s^{-1}
l	width of the basin, m
L	length of the basin, m
L_k	interfacial transfer of concentration between the two phases, $\mathrm{kg\,m}^{-3}\,\mathrm{s}^{-1}$
m	coefficient linked to Henry's coefficient, dimensionless
M_k	local instantaneous interfacial momentum transfer, $\mathrm{kg\,m}^{-2}\,\mathrm{s}^{-2}$
M_{O_2}	molecular mass of O_2, $\mathrm{kg\,mol}^{-1}$
P_G	pressure in bubble, Pa
P_k	local statistical averaged phase pressure, $\mathrm{kg\,m}^{-1}\,\mathrm{s}^{-2}$
Q_{diff}	mean air flow rate per diffuser, $\mathrm{m}^3\,\mathrm{h}^{-1}$
Q_T	total air flow rate, $\mathrm{m}^3\,\mathrm{h}^{-1}$
R	gas constant, ($R = 8.314\,\mathrm{J\,mol}^{-1}\,\mathrm{K}^{-1}$)
T	temperature, °C
U_C	mean axial liquid velocity, $\mathrm{m\,s}^{-1}$
v_d	drift velocity, $\mathrm{m\,s}^{-1}$
v_k	local instantaneous phase velocity of phase k, $\mathrm{m\,s}^{-1}$

v'_k	local instantaneous turbulent component of phase velocity, $m\,s^{-1}$
V_r	relative velocity, $m\,s^{-1}$
y_e	volume fraction of oxygen in air, dimensionless
z	distance from the bottom of the tank, m

Greek letters

α_k	retention of phase k, dimensionless
ε	dissipation rate of the turbulent kinetic energy, $m^2\,s^{-3}$
μ_L	water viscosity, $kg\,m^{-1}\,s^{-1}$
ρ_k	density of phase k, $kg\,m^{-3}$
σ	superficial tension between air and liquid, $kg\,s^{-2}$
τ_k	viscous stress tensor in phase k, $kg\,m^{-1}\,s^{-2}$

Acknowledgements

The authors are grateful to the persons who were involved in the experimental measurements on full scale aeration tanks.

References

Bel Fdhila, R., Simonin, O., 1992. Eulerian prediction of turbulent bubbly flow downstream of a sudden pipe expansion. In: Workshop on Two-phase Flow Predictions, 30 March–2 April, Erlangen.

Chatellier, P., 1991. Simulation de l'hydrodynamique des chenaux d'oxydation par l'utilisation des équations de Navier–Stokes associées au modèle K–e: evaluation de la vitesse de circulation. Thèse de doctorat, INSA, Toulouse, 168pp. + annexes.

Clift, R., Grace, J.R., Weber, M.E., 1978. Bubbles, Drops and Particles. Academic Press, New York.

Cockx, A., Do-Quang, Z., Liné, A., Roustan, M., 1999. Use of computational fluid dynamics for simulating hydrodynamics and mass transfer in industrial ozonation towers. Chemical Engineering Science 54, 5085–5090.

Cockx, A., Do-Quang, Z., Audic, J.M., Liné, A., Roustan, M., 2001. Global and local mass transfer coefficients in waste water treatment process by computational fluid dynamics. Chemical Engineering and Processing 40, 187–194.

Djebbar, R., 1996. Etude hydrodynamique des réacteurs de type chenaux d'oxydation par la mécanique des fluides numérique. Post Doc, INSA, Toulouse.

Fayolle, Y., 2006. Modélisation de l'hydrodynamique et du transfert d'oxygène dans les chenaux d'aération. Thèse de doctorat, Ecole doctorale Transfert, Dynamique des Fluides, Energétique et Procédés, INSA de Toulouse, 295pp. + annexes.

Fayolle, Y., Gillot, S., Cockx, A., Roustan, M., Héduit, A., 2006. In situ local parameter measurements for CFD modelling to optimize aeration. In: 79th Annual Technical Exhibition and Conference WEFTEC'06, October 21–25, Dallas, USA, 12pp.

Gillot, S., Capela, S., Héduit, A., 2000. Effect of horizontal flow on oxygen transfer in clean water with surfactants. Water Research 34 (2), 678–683.

Gillot, S., Capela-Marsal, S., Carrand, G., Wouters-Wasiak, K., Baptiste, P., Héduit, A., 2005. Fine bubble aeration with EPDM membranes: conclusions from 15 years of practice. In: IWA Specialized Conference on Nutrient Management in Wastewater Treatment Processes and Recycle Streams, Krakow, Poland, pp. 607–616.

Groves, K.P., Daigger, G.T., Simpkin, T.J., Redmon, D.T., Ewing, L., 1992. Evaluation of oxygen transfer and alpha-factor on a variety of diffused aeration systems. Water Environment Research 64 (5), 691–698.

Higbie, R., 1935. The rate of absorption of a pure gas into a still liquid during short periods of exposure. Am. Inst. Chem. Eng. 365–389.

Hinze, J.O., 1975. Turbulence. Mcgraw-Hill, New York.

Ishii, M., 1975. Thermo-fluid Dynamic Theory of Two-phase Flow. Eyrolles, Paris.

Jupsin, H., Vasel, J.-L., 2002. Détermination du Cs dans des réacteurs aérés par insufflation. 4èmes Journées Francophones sur les Reacteurs Gaz–Liquide et Gaz–Liquide–Solide, p. 8.

Mueller, J.A., Boyle, W.C., Pöpel, H.J., 2002. Aeration: principle and practice. In: Water Quality Management Library Series, 353pp.

NF-EN-12255-15 (2004). Wastewater treatment plants—Part 15: measurements of the oxygen transfer in clean water in aeration tanks of activated sludge plants.

Schiller, L., Naumann, Z., 1938. A drag coefficient correlation. Z Ver Deutsch Ing. 77–318.

Simon, S., 2000. Etude d'un chenal d'oxydation par des approches globales et locales—hydrodynamique et transfert de matière. Thèse de doctorat, INSA, Toulouse, 188pp. + annexes.

Talvy, S., Cockx, A., Line, A., 2007. Modeling hydrodynamics of gas–liquid airlift reactor. A.I.Ch.E. Journal 53 (2), 335–353.

Vermande, S., Essemiani, K., Meinhold, J., De Traversay, C., Fonade, C., 2003. Trouble shooting of agitation in an oxidation ditch: applicability of hydraulic modeling. In: 76th Annual Technical Exhibition and Conference WEFTEC'03, October 11–15, Los Angeles, USA.

Vermande, S., Chaumaz, M., Marsal, S., Dumoulin, L., Essemiani, K., Meinhold, J., 2005. Modélisation numérique d'un bassin à grande profondeur. Récent progrès en Génie des Procédés 92, 8pp.

Wagner, M.R., Pöpel, H.J., 1998. Oxygen transfer and aeration efficiency—influence of diffuser submergence, diffuser density, and blower type. Water Science and Technology 38 (3), 1–6.